The Hypersonic Inflatable Aerodynamic Decelerator (HIAD) Mission Applications Study

David M. Bose[1], Richard Winski[2], and Jeremy Shidner[3]
Analytical Mechanics Associates, Inc
Hampton, VA 23666

Carlie Zumwalt[4]
NASA Johnson Space Center
Houston, TX 77058

Christopher O. Johnston[5], D.R. Komar[6], F. M. Cheatwood[7], and Stephen J. Hughes[8]
NASA Langley Research Center
Hampton, VA 23681

The objective of the HIAD Mission Applications Study is to quantify the benefits of HIAD infusion to the concept of operations of high priority exploration missions. Results of the study will identify the range of mission concepts ideally suited to HIADs and provide mission-pull to associated technology development programs while further advancing operational concepts associated with HIAD technology. A summary of Year 1 modeling and analysis results is presented covering missions focusing on Earth and Mars-based applications. Recommended HIAD scales are presented for near term and future mission opportunities and the associated environments (heating and structural loads) are described.

Nomenclature

ADB	Aerodatabase
AIAA	American Institute of Aeronautics and Astronautics
C	C programming language
CEV	Crew Exploration Vehicle
CFD	Computational Fluid Dynamics
CH4	Liquid Methane
DGB	Disk-Gap-Band
EDL	Entry, Descent, and Landing
EDL-SA	Entry, Descent, and Landing Systems Analysis
EFPA	Entry Flight Path Angle
EXAMINE	Exploration Architecture Model for IN-space and Earth-to-orbit
FPA	Flight Path Angle
FSD	Flexible Systems Development
GRAM	Global Reference Atmospheric Model
HARA	High-temperature Aerothermodynamic RAdiation
HEART	High-Energy Atmospheric Reentry Test
HIAD	Hypersonic Inflatable Aerodynamic Decelerator
IEEE	Institute of Electrical and Electronics Engineers
IRVE	Inflatable Reentry Vehicle Experiment
L/D	Lift to Drag Ratio
L2	Earth-moon Lagrange Point 2
LAURA	Langley Aerothermodynamic Upwind Relaxation Algorithm
LEO	Low Earth Orbit
LFE	Lander Functional Element
LO2	Liquid Oxygen
MLI	Multi-Layer Insulation
MMH	Monomethylhydrazine
MOLA	Mars Orbiter Laser Altimeter
MPCV	Multi-Purpose Crew Vehicle
MSC	Marshal Spaceflight Center
MSL	Mars Science Laboratory
NASA	National Aeronautics and Space Administration
NTO	Nitrogen Tetroxide
Orion	The NASA Crew Exploration Vehicle Development Program
POST2	Program to Optimize Simulated Trajectories II
RCS	Reaction Control System
SRP	Supersonic Retro-Propulsion
TPS	Thermal Protection System

1. Vice President, Modeling and Simulation, 5500 Democracy Drive, Suite 110, Plano, TX, AIAA Senior Member
2. Engineer IV, Dynamics and Controls, 303 Butler Farm Road, Suite 104A, Hampton, VA, AIAA Senior Member
3. Supervising Engineer, Dynamics and Controls, 303 Butler Farm Road, Suite 104A, Hampton, VA, AIAA Senior Member
4. Aerospace Engineer, Flight Mechanics and Trajectory Design Branch, Mail Stop EG5
5. Aerospace Engineer, Aerothermodynamics Branch, Mail Stop 408A, AIAA Member
6. Senior Aerospace Engineer, Vehicle Analysis Branch, Mail Stop E401
7. EDL Principle Investigator, Space Technology Mission Directorate, Mail Stop 250, AIAA Associate Fellow
8. HIAD Chief Engineer, Mechanical Systems Branch, Mail Stop 432, AIAA Member

I. Introduction

The successful flights of the Inflatable Reentry Vehicle Experiment (IRVE)-2 and IRVE-3 projects have demonstrated the potential value of Hypersonic Inflatable Aerodynamic Decelerator (HIAD) technology. The development of this technology is currently pursued by the HIAD Project, funded by NASA's Office of Chief Technologist's Game Changing Program. The HIAD Project is divided into three areas, namely Flexible Systems Development (FSD), Flight Validation, and Advanced Entry Concepts. FSD has two elements including a Flexible Thermal Protection System (TPS) element and an Inflatable Structures element. The Advanced Entry Concepts effort is divided into Mission Applications and Next Generation Subsystems. Next Generation Subsystems is investigating methods for generating lift on blunted cones focusing on aerodynamic trim surfaces. Mission Applications is evaluating and developing concepts (including payload interfaces) for missions at multiple destinations for the purpose of demonstrating the benefits and need for HIAD technology. Providing a summary of concepts evaluated in Year 1 of HIAD Mission Application trade studies is the purpose of this paper. A more complete overview of the HIAD project is provided by Hughes et al.[1]

A. HIAD Mission Applications Overview

The objective of HIAD Mission Applications is to identify the improvements associated with HIAD integration within the concept of operations of high priority missions. Potential improvements may come in the form of performance, cost, or risk measures in all phases of the mission from spacecraft and launch vehicle integration through entry descent and landing (EDL). Some specific examples of potential improvements include:

- **Reduced launch costs**: can mass and/or packaging advantages of a HIAD allow for launch on smaller class of launch vehicle?
- **Enhanced Integration**: does HIAD packaging provide improved access to the payload and spacecraft subsystems during integration?
- **Increased performance margins**: does the increased deceleration of the HIAD allow for longer mission time between significant EDL events? Does a HIAD allow for a steeper entry angle, resulting in a smaller landing footprint?
- **Expanded mission potential and science return**: does HIAD integration lead to the ability to deliver more payload to the surface of the target destination and provide accessibility to higher altitude landing sites?

In order to uncover these benefits it is necessary to develop a full-systems view of HIAD integration. Performing this level of design and analysis is also an objective of HIAD Mission Applications. In addition, the development of results which can help to uncover system sensitivities, address what-if scenarios, and help guide future investments is a significant project goal. This includes, for example, understanding which secondary deceleration devices (supersonic parachute, subsonic parachute, supersonic aerodynamic decelerator, retro-propulsion) and landing systems (legs, air bags, crushable materials) make the most sense to couple with the HIAD for a given reference mission.

B. HIAD Mission Applications Approach and Scope

In order to address the objectives of HIAD Mission Applications, a work plan was crafted that calls for iterative modeling and analysis cycles with two levels of fidelity. The first is a conceptual level, characterized by trade studies aimed at identifying the required HIAD scale for missions of interest over a broad range of entry conditions. Typical trade parameters include entry flight path angle (EFPA), entry velocity, entry mass, and HIAD diameter. In a given analysis run, iteration on HIAD mass is required to ensure the mass-scaling of the HIAD is commensurate with the heat load and dynamic pressure associated with the flight trajectory. Once the trade is complete, recommended HIAD scale can be evaluated through application of system constraints (e.g. heat rate limits) to identify regions of feasibility. From the region of feasibility, design points are selected based on mission improvement objectives. The second level of fidelity provides deeper modeling and analysis activities into specific design points within the trade space. This "deep dive" roots out significant system drivers and develops a complete systems view of the design.

In Year 1 of HIAD Mission Applications, conceptual level trades were performed in the following areas. Selection of design points and "deep-dive" design and analysis is part of the Year 2 plan.

- **Hybrid Lunar Return**: evaluation of a HIAD in returning the Multi-Purpose Crew Vehicle (MPCV) from a lunar mission via direct Earth entry. This is considered a hybrid since the HIAD is used to augment the existing MPCV heat shield.
- **Hybrid Mars Return**: evaluation of a HIAD in returning MPCV from a Mars mission via direct Earth entry.
- **Launch Asset Recovery**: evaluation of a HIAD in the recovery of launch vehicle assets. This particular study focuses on 1st and 2nd stage recovery.
- **L2 to LEO Transfer**: evaluation of a HIAD in the transfer of the MPCV from an L2 Earth-Moon Lagrange point (L2) to a Low Earth Orbit (LEO) orbit through aerocapture.
- **Mars Fast Transit**: evaluation of a HIAD in the transfer of MPCV to low or high Earth orbits in a Mars fast transit scenario.
- **Mars Aerocapture**: evaluation of a HIAD in performing aerocapture at Mars.
- **Mars Southern Highlands**: evaluation of a HIAD in performing direct-entry at Mars with access to higher altitudes such as those associated with the Mars Southern Highlands region.

II. Modeling

A. Reference Vehicles

Two reference entry vehicles were employed in the studies conducted in Year 1. This includes a hybrid vehicle comprised of a HIAD affixed to the MPCV. The second is a standard 60 deg. sphere cone. High level attributes of these vehicles are described here. Mission specific vehicle attributes are called out in each study summarized in Section III. HIAD diameter, entry mass, entry velocity, and EFPA vary by application.

The "hybrid" reference vehicle combines a 60-degree HIAD with the MPCV. An artist's rendition of this concept is illustrated in Figure 1. The slope of the MPCV at the shoulder of the heat shield is roughly 67-degrees. As a result, a slope discontinuity exists between the heat shield and the HIAD. The impact of this is seen in aeroheating analysis, which predicts higher localized heating in the region of this discontinuity. It is assumed that detailed design of the MPCV/HIAD interface can mitigate these effects.

Hybrid Reference Vehicle
MPCV Diameter [m]: 5.0
Nose Radius [m]: 6.0
HIAD ½ Cone Angle [deg]: 60

Standard Vehicle
Nose Radius [m]: 4.0
HIAD ½ Cone Angle [deg]: 60 deg.

Figure 1. The hybrid reference vehicle.

B. Mass Model

Mass modeling of entry systems investigated in the studies summarized in Section III followed the Entry Descent and Landing Systems Analysis project (EDL-SA) approach[2,3], which provides a parametric mass model that mathematically represents mass components as a function of vehicle dimensions and key mission environmental

parameters such as maximum dynamic pressure and total heat load. EDL-SA mass models provided the foundation of the mass model employed in Year 1 studies. Improvements were made in the area of supersonic retro-propulsion as described in II.E.

C. Aerodynamics

Aerodynamic models for Year 1 HIAD Mission Applications were derived from the HEART (High-Energy Atmospheric Reentry Test) aerodatabase (ADB)[4,5]. The original baseline HEART entry vehicle is based on a 55° half-angle, 8.5 meter HIAD, and is designed for an Earth entry from LEO. CFD solutions for HEART were computed on a geometry which employed a low-profile ellipsoidal nose in order to meet launch vehicle packaging constraints.

The HEART aerodatabase is composed of three essential parts including free molecular HEART solutions at LEO conditions, continuum HEART solutions along a notional LEO entry from Mach 25 down to Mach 3, and super-/trans-/subsonic aerodynamics from the IRVE aerodatabase[6]. IRVE aerodynamics in the HEART ADB was taken from IRVE ballistic range testing and subsonic wind tunnel tests on the Moonrise configuration. Bridging functions are used to blend between aerodynamics from each ADB component and interpolations are performed using Mars Pathfinder heritage subroutines. Where applicable, correction factors are used to account for differing cone angles between configurations.

For the first stage launch vehicle recovery study, the HEART aerodynamics model was deemed inappropriate because these vehicles fly trajectories of a different type. Whereas the launch vehicle booster follows a parabolic ascent-descent trajectory which never exceeds Mach 10, HEART makes atmospheric interface at a Mach number of approximately 25. For these reasons, the IRVE ADB is used in the launch asset recovery study so that aerodynamics from a similar flight profile and regime are employed.

D. Aeroheating

Radiative and convective heating tables were compiled as a function of velocity and density for both Earth and Mars atmospheric compositions. The heating values in these tables were computed using state-of-the-art coupled LAURA-HARA simulations. The LAURA (Langley Aerothermodynamic Upwind Relaxation Algorithm) flowfield code is a high fidelity, structured grid analysis tool, specialized for hypersonic re-entry physics, utilizing state-of-art algorithms for computational fluid dynamic (CFD) simulations[7,8]. A two-temperature thermochemical nonequilibrium model is applied in LAURA. The shock-layer radiation is modeled with the HARA (High-temperature Aerothermodynamic RAdiation) code[9,10]. HARA treats the non-Boltzmann radiation of atomic and molecular species. The divergence of the radiative flux, computed using the tangent slab approximation, provides the coupling between HARA and LAURA[11].

The treatment of thermochemical nonequilibrium effects in the LAURA flowfield solution and non-Boltzmann modeling in the HARA radiation solution represent significant modeling improvements over the widely used Sutton-Graves convective heating correlation and Sutton-Hartung[12,13] radiative heating tables (or Tauber-Sutton correlations[14]). The heating tables for Earth and Mars entries computed in the present work are discussed in the following two subsections and compared with the previous models.

D.1 Earth-based Model

The Earth-based studies considered in this work were focused on the hybrid entry vehicle (MPCV-HIAD). To simplify this geometry for computing the hundreds of cases required for the heating tables, a 60-degree sphere-cone with a 6.035-m nose radius and maximum diameter of 14m was considered. There are only slight differences between this simplified geometry and that of the hybrid vehicle. The 11-species thermochemical nonequilibrium model for air[15,16] was applied for these Earth entry studies. The convective heating was assumed fully turbulent using the Cebeci-Smith model and the wall was assumed super-catalytic. Based on the study by Johnston et al.[17], the radiative heating margin of 44% for velocities less than 13 km/s and 74% for velocities greater than 13 km/s are recommended. For the convective heating, a margin of 40% is recommended. Convective and radiative heating estimates as a function of density and velocity are illustrated in Figure 2 and Figure 3, respectively.

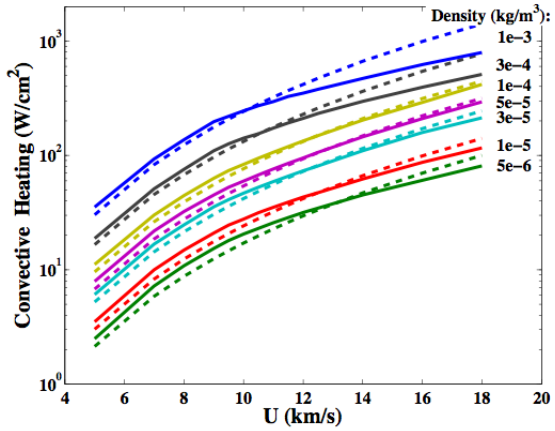

Figure 2. Convective heating comparison between present model (solid) and Sutton-Graves (dashed)

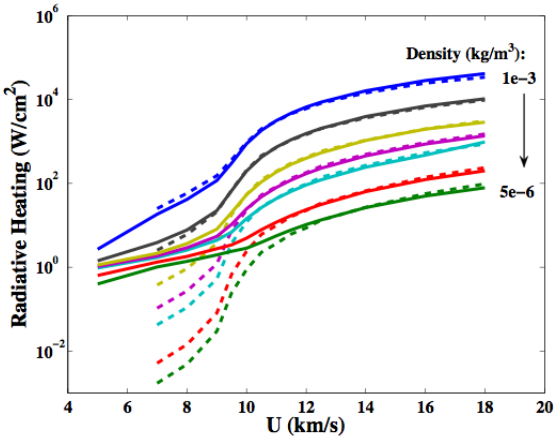

Figure 3. Radiative heating comparison between present model (solid) and Sutton-Hartung (dashed)

D.2 Mars-based Model

The Mars-based studies considered in this work were focused on a 60-degree sphere-cone with a 4.0m nose radius and maximum diameter of 12m. The chemical kinetics and radiation models applied in these simulations are taken from Johnston et al [18]. Based on this study, the radiative heating margin of 50% and convective heating margin of 40% is recommended.

Aeroheating analysis in support of Year 1 studies included analysis of sensitivity to a number of assumptions including the catalycity of the materials, angle of attack, HIAD diameter, and flow conditions (laminar vs. turbulent). In general, a significant reduction (up to 60%) in the convective heating results with a non-catalytic material vs. super-catalytic at higher entry speeds. Although predicted heating profiles will vary with HIAD diameter, angle of attack and flow conditions, the use of stagnation point heating as a proxy for heating across the HIAD was found to be a conservative assumption for angles of attack less than 15 degrees. In consideration of these sensitivity studies, stagnation point heating tables with margins applied are used as the basis for the heating estimates reported in each of the Year 1 studies. In select studies, super-catalytic and non-catalytic heating tables were both exercised in order to explicitly estimate the impact of this assumption on recommended HIAD sizing.

E. Supersonic Retro-Propulsion Mass Modeling

The objective of the supersonic retro-propulsion mass modeling effort was to develop a scalable, parametric mass model for the supersonic retro-propulsion (SRP) stage and lander functional element (LFE) to support the integrated EDL performance analysis conducted in the Year 1 studies. The SRP includes all of the functions required for descent and terminal landing propulsion, while the LFE included all other functions required by the integrated system at terminal landing. This functional element split allows various terminal landing options to be readily traded.

The Exploration Architecture Model for IN-space and Earth-to-orbit (EXAMINE)[19] modeling framework, developed in-house at NASA Langley Research Center, was used to model the mission events and develop the parametric mass estimates of the SRP and LFE. The parametric models are used to generate response surface equations that are incorporated directly into the flight performance simulation, as demonstrated in previous EDL study efforts[20].

E.1 SRP Model

Mono-propellant hydrazine was not considered for this study. Bi-propellant systems considered included the following four options:

1. Pump-fed engine burning nitrogen tetroxide (NTO) and monomethylhydrazine (MMH)
2. Pressure-fed engine burning NTO and MMH
3. Pump-fed engine burning liquid oxygen (LO2) and liquid methane (CH4)
4. Pressure-fed engine burning LO2 and CH4

The primary SRP stage structure is modeled as a 2.6 m diameter aluminum-lithium cylinder that supports the tank system and payload. This primary structure mass is estimated from a historically-based empirical curve fit [21]. Thrust structure mass is based on a historical fit accounting for stage diameter, the number of engines and the thrust load. Secondary structure mass is 5% of the primary plus thrust structure masses.

The reaction control system (RCS) has sixteen pressure-fed thrusters each producing a thrust of 100 lbf. Each thruster operates at a chamber pressure of 125 psia, a mixture ratio of 1.65, and an area ratio of 40 delivering an Isp of 301.3 sec. The RCS propellants are stored at 225 psia in two spherical graphite-wrapped aluminum tanks, one for NTO and one for MMH. Tank heaters and 10 layers of multi-layer insulation (MLI) provide thermal control for the tanks during interplanetary coast while a 6,000 psia gaseous helium tank, constructed of graphite-wrapped aluminum, provides consumables for RCS tank pressurization.

Thermal control for SRP vehicle systems includes MLI, heaters and a heat pipe heat rejection system. The mass estimate for the SRP thermal control system is derived from the Mars Science Laboratory project (MSL). In addition, mass estimate for cabling, instrumentation and stage separation pyro-bolt mechanisms were derived from MSL.

Ground rules of the EDL Feed Forward study, conducted under EDL-SA, required a total mass margin of 49.5% of the basic dry mass which includes allocations for both mass growth allowance and project manager's reserve.

E.2 Lander Functional Element

The LFE mass model includes the common and dedicated functional subsystems for the various landing mode trade options considered. For common function subsystems, mass estimates are derived directly from MSL. For the optional subsystems, a basic parametric approach was utilized initially while more detailed models are developed. Landing leg and airbag system masses are determined parametrically as a function of landed mass. Typical values for landing legs range from 2-5% of the landed mass, although small robotic-class landers using landing legs could potentially have a higher landing leg fraction[22]. For landing airbags, a range of 1-5% is typical. As a point of reference, a land landing study for the Orion capsule was performed and the resulting landing airbag fraction was approximately 2.5% [23]. For robotic-class missions with smaller landed mass the airbag fraction could be a higher fraction of the mass.

F. Flexible Thermal Protection System

Advances in flexible TPS are being pursued though the Flexible Systems Development element of the HIAD Project. This includes a detailed test program for material layups as well as the development and calibration of a high fidelity thermal model for predicting TPS performance in a real mission configuration and environment. Application of this high fidelity model will be performed as part of the deep dive design and analysis activity planned under Year 2 of HIAD Mission Applications. In Year 1, however, consideration for flexible TPS is made in the application of TPS performance limits as constraints to trade study results. At the current time, these limits are based on the performance targets of the Flexible Systems Development element. These targets include:

- 1st Generation Flexible TPS, targeting a 5-meter HIAD: 20 W/cm^2
- 1st Generation Flexible TPS, targeting a 10-meter HIAD: 30 W/cm^2
- 2nd Generation Flexible TPS, targeting a 10-meter HIAD: 50 W/cm^2
- 3rd Generation Flexible TPS, targeting a 10-meter HIAD: 75 W/cm^2

G. Simulation Development

In order to simulate a broad range of potential HIAD applications, a simulation framework was needed that would work across multiple planets and mission scenarios. The Program to Optimize Simulated Trajectories II (POST2) was selected as the primary simulation tool. The latest version 3.0 was upgraded as needed in the HIAD Mission Applications study. The benefits of using this latest version include the program being written in C, stability of the code base, and improved source code control. An additional benefit that POST2 offers is a diverse selection of atmosphere models. All of the Marshall atmosphere models, denoted GRAM (Global Reference Atmospheric Model), have been incorporated and checked out in POST2. This provides a baseline atmosphere to use for multiple planets including Earth, Mars, Venus, Titan and more.

III. Year 1 Trade Studies

Studies performed in support of Year 1 HIAD Mission Applications activities are summarized in this section.

A. Hybrid Lunar and Mars Return Studies

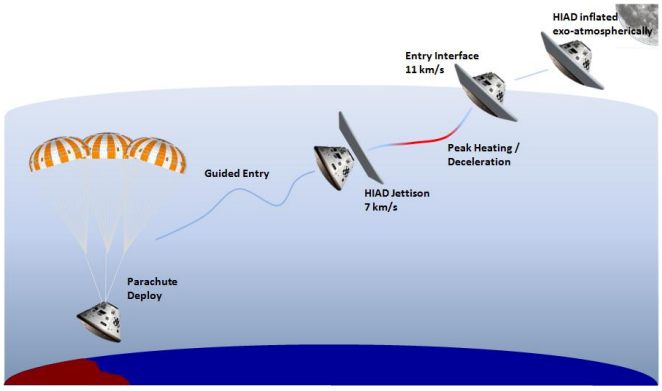

Figure 4. Hybrid lunar return concept of operations.

Return from lunar orbit must deal with higher energy entries than that from typical LEO return. Entry velocities from lunar return increase from approximately 8 km/s from LEO to 11 km/s. Heat shield technology must address these higher energy states. The Hybrid Lunar Return study explores whether the addition of a HIAD could effectively allow a lunar return to fly an environment profile similar to that of a LEO return. The approach for placing the lunar return capsule on a LEO return trajectory is to utilize a HIAD to reduce the system energy initially, jettison the HIAD at a specified velocity, then fly a guided trajectory to the target. The nominal concept of operations is shown in Figure 4, where the HIAD is inflated exo-atmospherically, entry interface occurs at an inertial velocity of 11 km/s, the HIAD is jettisoned at 7 km/s, and the rigid capsule continues along the trajectory utilizing an MPCV-like center-of-mass offset to generate lift for guided entry, culminating in parachute deploy.

A.1 Setup and Assumptions

The entry aerodynamics model utilizes the adjusted HEART aerodatabase as described in Section II.C. At HIAD jettison, the Orion aerodatabase, v0.54 is utilized. The aeroheating calculation for the hybrid entry vehicle was included with margins as detailed in Section II.D. The MPCV aeroheating utilized values from the CEV Aeroscience Project's assessment of MPCV heating for both convective and radiative values with margins of 1.35 and 2.0, respectively.

A trade space of HIAD diameters from 8 to 20 meters and jettison velocities from 6 to 8 km/s was investigated. The trajectory is shaped by varying the entry flight path angle to achieve a desired peak loft during the HIAD phase of flight. For many cases, the HIAD jettison would provide a useful abort to orbit capability if the jettison occurs early enough. By jettisoning the HIAD, the increase in ballistic coefficient (300 kg/m^2) reduces the flight path angle variation over a given time, enabling abort. However, by lofting too greatly with the HIAD, the rigid MPCV may not have enough control authority to effectively capture into the atmosphere (i.e. result in a skip out). This creates a tradeoff between increased heating/reduced lofting and reduced heating/increased lofting. The trade space examined peak lofting values of 0 to -2 degrees.

A.2 Results and Conclusions

Results were investigated by first establishing a lunar return baseline. Two trajectories were created, the first using a similar bank profile as flown on the Apollo 11 lunar return[24], but with MPCV shape and mass parameters. The second trajectory utilized a bank profile derived from Orion's skip-entry guidance. The difference between the two trajectories is the peak lofting allowed. The skip-entry guidance allows greater lofting, which helps to reduce heat rate and g-load by removing less energy during the initial atmospheric dive. The Apollo lunar return trajectory does not allow as much lofting, thereby resulting in higher g-loads and heat rate.

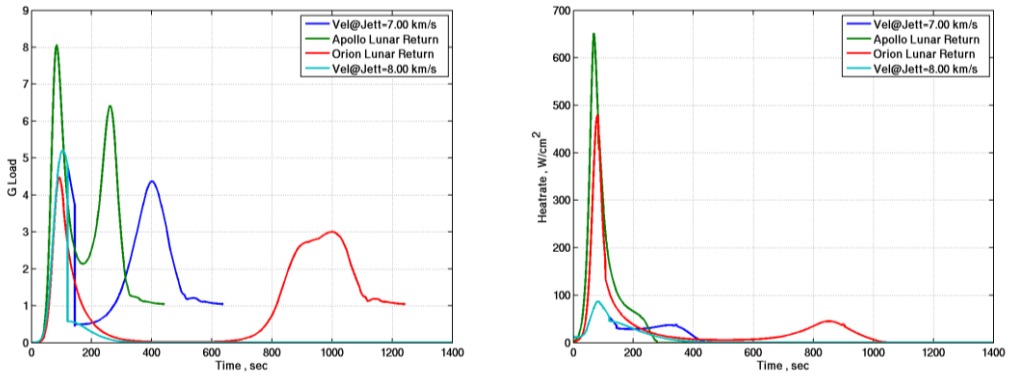

Figure 5. Baseline trajectory comparisons.

The baseline trajectories are plotted in Figure 5. Heat rate includes both convective and radiative components. The green line represents the Apollo lunar return, the red line represents the Orion lunar skip return, the blue line represents the nominal hybrid lunar return trajectory and the cyan line represents an abort to orbit case for the hybrid lunar return. The hybrid lunar return trajectory utilizes a 15 meter HIAD and peak loft of 0 degrees. Jettison of the HIAD occurs at 143 seconds, corresponding to a planet relative velocity of 7 km/s. The g-loads remain similar to the Orion skip entry return, but only utilize half the flight time. The velocity required to safely abort for the hybrid lunar return case is 8 km/s. There is approximately 87 seconds from a sensed g-load of 0.1 to the 8 km/s jettison velocity, during which the vehicle can determine if there is a need to abort, with 24 seconds remaining before the nominal jettison of 7 km/s.

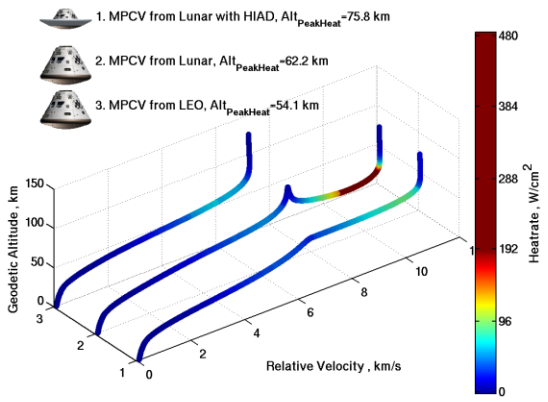

Figure 6. Hybrid lunar return altitude, velocity and aeroheating profile comparisons.

Results indicate that a HIAD of 18 meters is required to achieve a peak heat rate that falls below the HIAD G3 TPS limit of 75 W/cm^2. Mass of the 18 meter HIAD is approximately 18% of the 9 MT MPCV mass. Radiative heating is seen to contribute to only 20% of the peak heating.

Figure 6 depicts a side-by-side comparison of the hybrid lunar return trajectory (1), Orion skip-entry (2), and an Orion return from low Earth orbit (3). The lines are colored by peak heat rate and plotted against planet relative velocity verses geodetic altitude. The hybrid lunar return effectively creates a trajectory that looks very similar in heating to the MPCV trajectory returning from low Earth orbit. This reduction could remove the need for new TPS material to handle the high heating of the Orion skip-entry trajectory.

A.3 Hybrid Mars Return

A Mars return scenario must deal with higher energy entries than that associated with lunar return. Entry velocities of vehicles returning from Mars increase from 11 km/s as assumed in the Lunar Return study to 13.5 km/s for the Mars Return study. The approach and analysis setup investigated for returning the Mars vehicle to Earth is the same as used in the Hybrid Lunar Return study, however, the mass is increased from 9 metric tons to 15 metric tons to accommodate the assumed increase in return mass from a Mars mission.

Results, assuming a peak loft of 0.5 degrees show that for a HIAD of 14.5 meters, the radiative heat rate is two thirds of the total heat rate of 750 W/cm^2, with a HIAD system mass of 1800 kilograms, or about 12% of the MPC-alone mass. The high radiative heat rate is expected as the entry velocity increases. As the HIAD diameter increases, heat rates are lowered, however, the design is moving closer to the skip out boundary. For the HIAD diameters of 8 to 20 meters investigated, there were no cases below the 3rd generation flexible TPS target of 75 W/cm^2.

C. Launch Asset Recovery

Recovery of launch vehicle assets has the potential to reduce the overall cost of launch services while avoiding further proliferation of orbital space debris. The Launch Asset Recovery Study provided a quick look at potential benefits of a HIAD in recovering launch vehicle assets. The approach taken is to use a HIAD to enable recovery by delivering the asset to a subsonic chute deploy condition, similar to that of NASA's MPCV parachute system. The case study analyzed is for a two-stage to orbit launch vehicle, but is applicable to other launch vehicles.

C.1 Setup and Assumptions

The concept of operations is shown in Figure 7. The launch vehicle profile is a two-stage to orbit. At first stage separation, the second stage continues thrusting while the first stage lofts to an altitude of 225 km. The engine cutoff, loft and fall back to Earth occur over a period of 350 seconds before reentering the atmosphere. At this time, the HIAD inflates around the first stage as it reorients. First stage reentry occurs at a relative velocity of 3 km/s and a 30 degree entry flight path angle. The second stage achieves low earth orbit of 300 km altitude at which point the payload is separated. The second stage then deorbits, inflating the HIAD after the burn, but prior to entry interface.

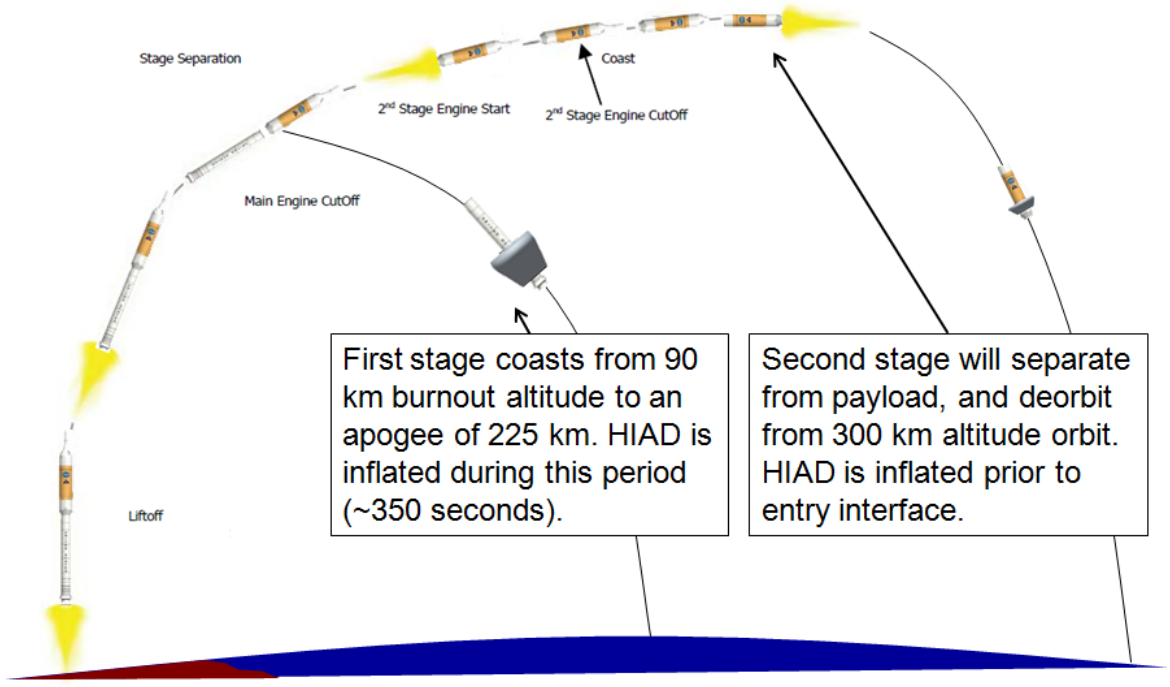

Figure 7. Launch asset recovery concept of operations.

The analysis assumes a trade space in mass for the first stage of 19 to 22 metric tons and second stage of 3 to 4 metric tons. The trade space varies initial velocity by 500 m/s of the first stage and a deorbit delta-v of 100 to 500 m/s of the second stage. HIAD diameter is varied in the trade space by 3.5 to 15 meters for the first stage and 3.5 to 10 meters for the second stage.

C.2 Results and Conclusions

Results were investigated in terms of ballistic coefficient, in order to capture the mass to diameter relationship. The final results are related to parachute deploy conditions of the MPCV parachute system, which is given in Mach verses altitude space. Figure 8 shows contours of ballistic coefficient and dynamic pressure of the first stage, where paths can be traced through Mach and altitude space. A subplot is shown in Figure 8 that maps ballistic coefficient to HIAD diameter for this study. The addition of a 10 meter HIAD to the first stage reduces the ballistic coefficient from a no HIAD value of approximately 1300 kg/m^2 to 200 kg/m^2, helping to achieve a trajectory that passes through the MPCV chute deploy box, and also reduce the dynamic pressure at which the parachute must operate.

The ballistic coefficient of the second stage without the HIAD is approximately 240 kg/m^2, which achieves a trajectory capable of entering the MPCV chute deploy box, albeit with less margin to dispersions. Including a 5-meter HIAD places the vehicle in a location that retains chute deploy margin.

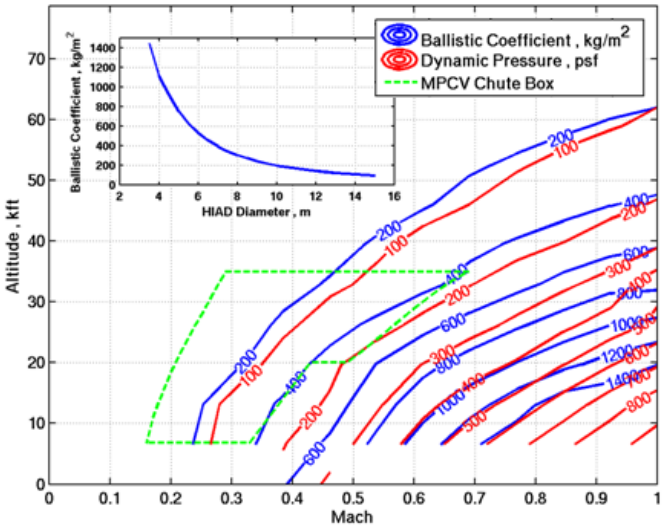

Figure 8. First stage trade space, parachute deploy conditions.

D. Aerocapture Studies: L2 to LEO Transfer, Mars Fast Transit, and Mars Aerocapture

Three studies, two at Earth and one at Mars, were completed to assess the feasibility of using HIADs in potential aerocapture mission scenarios. A parametric analysis was completed in each study to determine the sensitivity of HIAD scale to changes in input parameters such as target orbit and arrival velocity. For each study, a set of trade parameters were defined and then permutations of each parameter were used to create individual runs. The entry corridor was calculated for each run to provide insight into the heating environment experienced by each permutation. Ultimately, a recommended HIAD scale was reported which satisfies desired performance requirements.

The entry corridor is defined by flying one trajectory lift vector up the entire pass and one trajectory lift vector down the entire pass, then iterating on the EFPA that allows each trajectory to achieve the desired apoapsis. The two resulting entry flight path angle values provide a boundary, where any value less than the shallow side of the corridor results in a case that hits too high of an apoapsis or skips out of the atmosphere and any value greater than the steep side of the corridor results in case that hits too low of an apoapsis or impacts the surface. The two sides of the corridor provide information on the range of specific trajectory parameters, such as heat rate and g-load, expected within the corridor.

D.1 Setup and Assumptions

Each study was evaluated using a 3 degree of freedom simulation in POST2. The reference vehicle for the Earth-based studies was the hybrid vehicle. For the Mars-based study the standard reference vehicle was assumed. Heat rate was estimated using the models described in Section II.D with margins. The mass of the HIAD was estimated using the EDL-SA model. The model receives HIAD diameter and dynamic pressure as inputs and is valid for

diameters ranging from 8 to 20m and dynamic pressure between 500 and 5000Pa. For the Earth-based studies the atmosphere is modeled using the 1976 standard atmosphere tables, and for the Mars-based study the atmosphere is modeled using the 2005 Mars GRAM.

D.2 L2 to LEO Transfer

The L2 to LEO transfer study focuses on the addition of a HIAD to the MPCV in order to enable aerocapture into a LEO orbit from L2 return speeds. The list of inputs and trade parameters are given in Table 1, where the 9mT capsule mass value approximates the MPCV design and does not include the mass of the HIAD. This combination of input parameters produces cases with ballistic number ranging between 18 and 50 kg/m^2.

Table 1. Trade parameters for L2 to LEO transfer study.

Parameter	Value/Range Studied
Lift-to-Drag	0.05 to 0.20
Arrival Velocity	11.5 km/s
Target Orbit	400 km Circular
Capsule Mass	9 mT
Aeroshell Diameter	15 to 25 m

Corridor width remains nearly constant with changing HIAD diameter, but grows with an increase in L/D. While changing the diameter of the HIAD does change the entry flight path angle required to achieve the target apogee, it does not change the width of the entry corridor. Rather, it shifts the entire corridor higher in the atmosphere for a larger HIAD, and lower in the atmosphere for a smaller HIAD. From past Earth-based studies, about 0.5 degree of entry corridor width is required for an aerocapture mission to be flyable in consideration of uncertainties. By this threshold, 0.10 L/D cases are on the cusp of being flyable. An L/D of at least 0.15 is recommended.

Figure 9 shows the peak total heat rate associated with entry corridors representative of the study trade space. Basing the worst case heat rate from the average of the peak total heat rate values from the steep and shallow sides of the corridors, and considering the 3rd generation flexible TPS performance target of 75 W/cm^2, a HIAD diameter of approximately 23m is required for this mission.

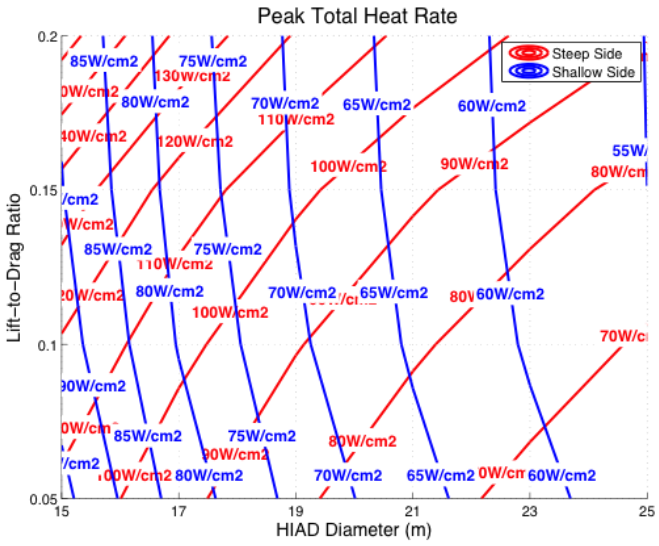

Figure 9. Peak total heat rate values for each side of the entry corridor.

D.3 Mars Fast Transit

The Mars Fast Transit study focuses on the use of a HIAD for Earth aerocapture from Mars return. The list of inputs and trade parameters are given in Table 2, and this combination of input parameters produces cases with ballistic number ranging between 10 and 430 kg/m^2. Note that the capsule mass does not include the mass of the HIAD.

Table 2. Trade parameters for Mars fast transit study.

Parameter	Value/Range Studied
Lift-to-Drag	0.05 to 0.20
Arrival Velocity	12 to 20 km/s
Target Orbit	400 km Circular (LEO) 233,850 x 407 km (HEO) 400,000 x 500 km (Lunar)
Capsule Mass	5 to 30 mT
Aeroshell Diameter	9 to 27 m

Identical to the previous study, each permutation of the inputs is examined to determine if sufficient corridor width is available and then a recommendation on HIAD scale is given based on peak heat rate limitations of the insulative TPS material.

The trade space for this study is very large but an analysis of the corridor width is able to quickly eliminate multiple cases. Analysis of corridor width across the trade space indicates that an L/D of 0.1 is sufficient for capturing the 400 km target orbit for all entry speeds investigated. It is possible to have a flyable mission with an L/D of 0.05 but entry speed in this case must be greater than 16 km/s. For the higher target orbits, entry speed must be higher than 15 km/s and L/D must be greater than 0.1 in order to have sufficient corridor.

Eliminating cases which do not satisfy the corridor width and do not have lower than 75 W/cm^2 of peak total heat rate leaves only the 12km/s entry speed and 400km apogee target combination. Within that, only the 5 and 10mT capsule mass combinations produce cases which satisfy the peak heat rate limit. Peak total heat rate contours for the 5 and 10mT cases are shown in Figure 10. Results indicate that a HIAD of at least 21m for the 5mT case, and 27m for the 10mT case are required to satisfy all constraints.

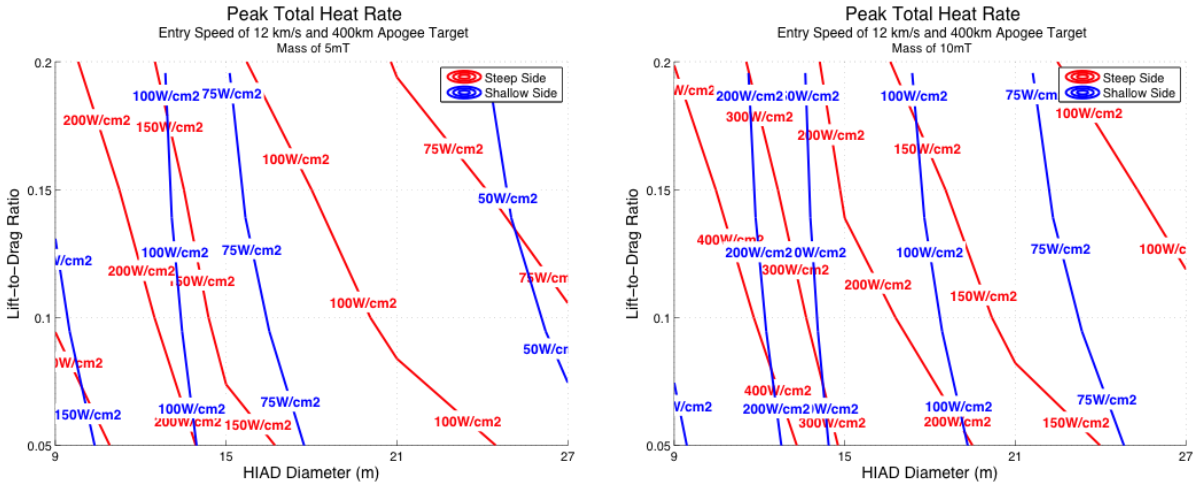

Figure 9. Peak total heat rate contours for the 5 and 10mT capsule mass cases.

One limitation in this analysis is the extensibility of the mass model. The model, which is designed for HIAD diameters ranging from 8 to 20m, is being used to analyze diameters as large as 27m. Additionally the model, which is designed to a maximum peak dynamic pressure of 5000 Pa, is receiving inputs of up to 150,000 Pa from the higher mass and entry speed cases. Such large extrapolation of the mass model results in an overestimation of HIAD mass. As the HIAD mass grows, the system mass grows, which forces the vehicle to fly a much steeper entry flight path angle to hit the target, resulting in a very high peak heat rate value. If the HIAD mass is overestimated, then the associated peak heat rate value and, more importantly, the recommended HIAD diameter may be as well.

D.4 Mars Aerocapture

The Mars aerocapture study focuses on the use of a HIAD to aerocapture into Mars orbit. The list of inputs and trade parameters are given in Table 3, and this combination of input parameters produces cases with ballistic number ranging between 4 and 329 kg/m^2. Note that the capsule mass does not include the mass of the HIAD.

Table 3. Trade parameters for the Mars aerocapture study.

Parameter	Value/Range Studied
Lift-to-Drag	0.05 to 0.20
Arrival Velocity	7.4 and 9.5 km/s
Target Orbit	500 km Circular 33,793 x 250 km (1 sol)
Capsule Mass	1 to 10 mT
Aeroshell Diameter	6 to 16 m

Uncertainties, for example in the initial state and atmospheric properties, are greater at Mars than at Earth. As a result, the amount of corridor width required to successfully aerocapture grows from 0.5 degree at Earth to roughly 1 degree at Mars. Analysis of corridor width across the trade space indicates that an L/D greater than 0.1 is required to make the 500 km target orbit flyable. The 1 sol target orbit requires even more L/D. In order to fly the full range of arrival velocities, an L/D closer to 0.2 is required.

Figure 11 focuses on the 10mT, 0.2 L/D results. Here, peak heat rate contours are plotted against entry speed and HIAD diameter. A HIAD of at least 9m is required for the 7.36 km/s entry speed case, and at least 26m for the 9.5 km/s entry speed case. These results assume super-catalytic materials in the aeroheating model. In the case of a non-catalytic assumption, it is possible to lower the recommended HIAD scale. For the 7.36 km/s entry speed case, the recommended scale lowers from 9m to 6m. For the 9.5 km/s entry speed, the recommended 26m lowers to 18m (roughly a 30% reduction in recommended HIAD scale).

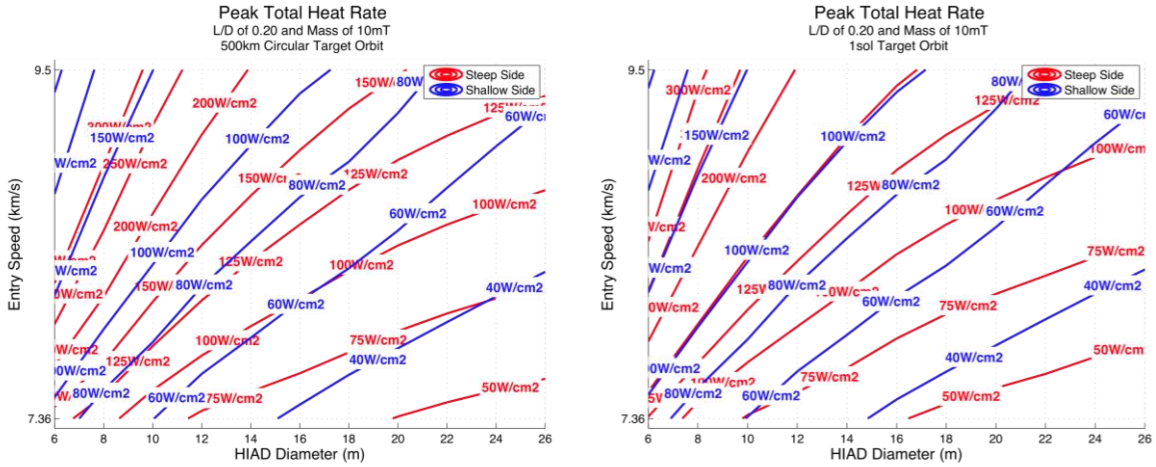

Figure 11. Peak heat rate values for the 500km circular and 1 sol target orbit results.

E. Mars Southern Highlands

The Mars Southern Highlands study explored the potential benefits of using a HIAD for direct entry, descent, and landing at Mars. A motivation for targeting the Southern Highlands is the evidence of groundwater in the region[25]. One of the challenges impeding missions to these sites is the elevation, which ranges from +1.5 to +3 km MOLA. As demonstrated in Figure 12, all previous Mars missions have landed at lower elevations.

The study examined multiple EDL architectures to determine feasibility of each while identifying staging conditions and possible benefits over current rigid body technology. The approach taken was to simulate a wide trade space and then apply constraints to eliminate non-viable cases. The maximum payload or landed mass case is then chosen from the remaining solutions.

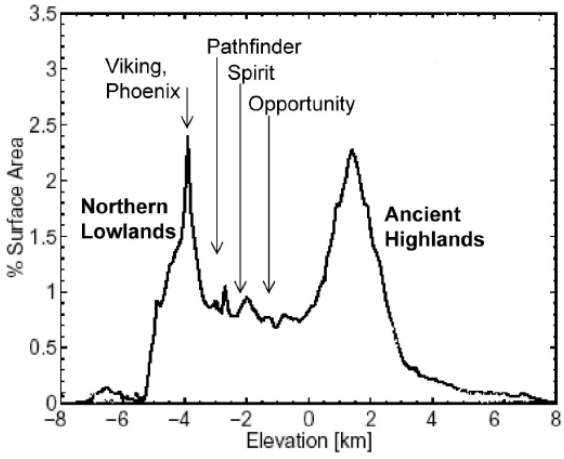

Figure 12. Mars elevation area distribution[26].

E.1 Setup and Assumptions

Parametric vehicle models were integrated into the POST2 simulation such that both trajectory characteristics and vehicle component masses were outputs of each simulation.

Table 4. List of Architectures proposed.

Architecture	Hypersonic	Supersonic	Subsonic	Comments
01.01.05	HIAD	HIAD	Parachute	Small mass systems
01.01.06	HIAD	HIAD	Retroprop.	
01.02.02	HIAD	Retroprop.	Retroprop.	SRP stage to ground
01.02.05	HIAD	Retroprop.	Retroprop.	SRP stage separates, landed stage has separate subsonic propulsion
01.03.00	HIAD	Parachute	-	Small mass systems, large parachute
01.03.06	HIAD	Parachute	Retroprop.	MSL-like
01.04.00	HIAD	Skirt	Retroprop.	Small mass systems, large skirt
01.04.06	HIAD	Skirt	Retroprop.	

All architectures were assumed to be ballistic with no guidance and control. This study also assumed a landing elevation of +4 km MOLA. A general 20 G (Earth G of 9.81 m/s^2) entry deceleration limit was applied. For comparison, MSL had a maximum of around 13 G. Table 4 lists the architectures that were explored. A numbering scheme is used to shorten the description where the first number corresponds to the hypersonic decelerator, the second number corresponds to the supersonic decelerator, and the third number corresponds to the subsonic decelerator selected for the architecture.

Within each architecture, many options were assessed. This included multiple engine types including NTO/MMH and LO2/CH4 bipropellant systems. For each, a pressure-fed and pump-fed option was evaluated. Other options included the engine area ratio.

E.2 Architecture 01.01.05

This architecture uses a HIAD through the hypersonic and supersonic phases. Staging is done in the subsonic regime where the vehicle is separated from the HIAD and uses a parachute to land on the surface. Table 5 lists the variables used in the trade space and the domain of each. Since the parachute is the only decelerator device, other than the vehicle drag itself, the upper end of the parachute diameter domain is large, larger than any used on previous Mars robotic missions. The parachute is assumed to be a disk-gap-band (DGB), the same type used on Viking, Mars Pathfinder, the Mars exploration rovers, Phoenix, and MSL.

Table 5. Trade space for architecture 01.01.05.

Variable	Low Value	High Value
HIAD Diameter, m	4.0	20
Entry Mass, kg	500	6000
Entry Flight Path Angle, deg	-12	-20
Entry Velocity, m/s (hyperbolic)	3500	6000
Parachute Diameter, m	15	35
Parachute Deployment Mach	0.5	0.9

For each point in the trade space, an optimal HIAD diameter was determined so as to maximize landed mass. However, landed mass results did not consider the mass of the landing attenuation system. Once incorporated into the results with associated constraints, there were no valid vehicle designs found.

There are multiple reasons for the failure to close on valid designs. This includes a limit enforced on landing velocity (20 m/s), which is difficult to achieve with just a DGB parachute and the entry masses considered. Additionally, there is a limit to the maximum stroke on the landing attenuation systems considered (airbags and crushable materials). Finally, there are limits to the crush load for the crushable system.

E.3 Architecture 01.01.06

This architecture uses a HIAD through the hypersonic and supersonic phases. Staging occurs in the subsonic regime where the vehicle is separated from the HIAD and uses retro-propulsion to land on the surface. Table 6 summarizes the trade space explored in this study. Additional assumptions were employed based off of the Phoenix project. Specifically, a landing velocity of 2.5 m/s, a throttle maximum of 80%, and a minimum of 1 km of altitude for powered descent are assumed. Further, the powered descent is assumed to be a gravity turn.

Multiple engine types were assessed through the propulsion and vehicle mass models. For this architecture, the pump-fed NTO/MMH bipropellant propulsion system resulted in the largest payload masses. In Figure 13, the trade space is not fully filled with viable solutions. The various constraints become active in different regions. For instance the 20 G entry deceleration limit is active along the bottom, where EFPA is steeper, while the 80% maximum throttle setting is active along the side for the lower velocity staging conditions. Note that the HIAD diameter increases rapidly as the Mach number decreases. The payload mass also falls rapidly since the HIAD has become a larger portion of the total vehicle mass. The drag coefficient of the HIAD decreases rapidly around Mach 1 and below, which makes the staging condition Mach number a primary driver of the HIAD diameter in this architecture. All the results shown here are based on a nominal analysis with constraints applied.

Table 6. Trade space for architecture 01.01.06.

Variable	Low Value	High Value
HIAD Diameter, m	4.0	30
Entry Mass, kg	1000	6000
Entry Flight Path Angle, deg	-12	-20
Entry Velocity, m/s (hyperbolic)	3500	6000
Engine Ignition Mach	0.3	0.9

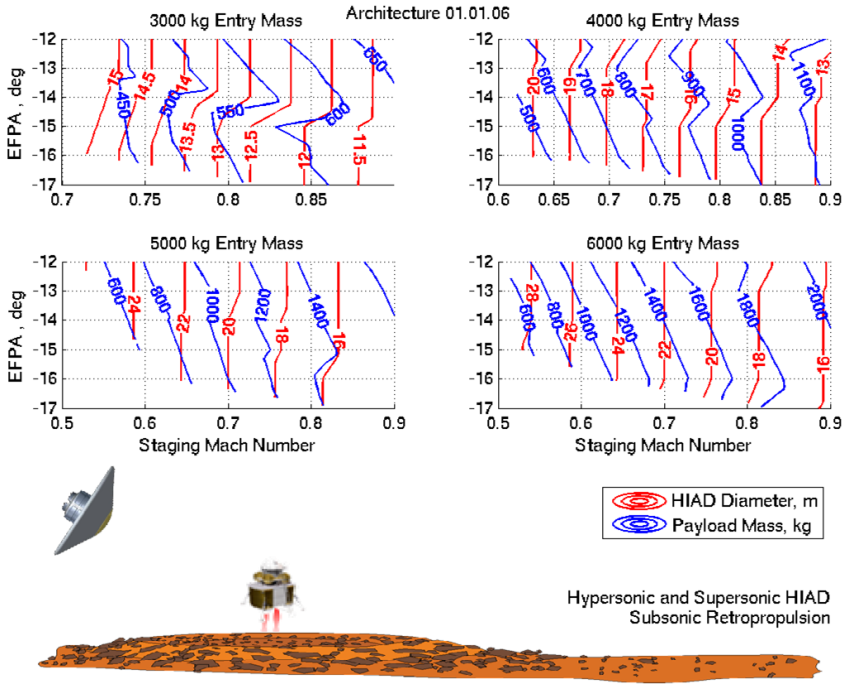

Figure 13. HIAD diameter and payload mass results.

E.4 Architecture 01.02.02

This architecture uses a HIAD through the hypersonic phase and into the supersonic phase. Staging is performed in the supersonic regime where the vehicle is separated from the HIAD and uses a retro-propulsion system, from supersonic through subsonic, to land on the surface. The trade space, retro-propulsion and landing constraints employed in architecture 01.01.06 were also employed here with one exception. Engine ignition Mach was explored over a range of Mach 1 to 3.

Figure 14 presents the optimal HIAD diameter and landed mass versus entry conditions. The largest difference with Architecture 01.01.06 is the smaller resulting HIAD sizes. This is primarily explained by the fact that the HIAD is more efficient in providing drag at supersonic conditions whereas the retro-propulsion is more efficient at subsonic speeds. This also explains the turning of the diameter contours as the staging Mach number approaches one. The trend towards a larger HIAD in the lower right corners of each contour plot is mainly driven by the EFPA and throttle setting. As the EFPA steepens, the altitude at the staging condition, given a constant diameter vehicle, will decrease. At some point the altitude is such that the maximum throttle setting comes against the limit. In response,

the HIAD diameter increases to provide the necessary deceleration. This sensitivity would change for a powered descent assumption different from the gravity turn assumed here.

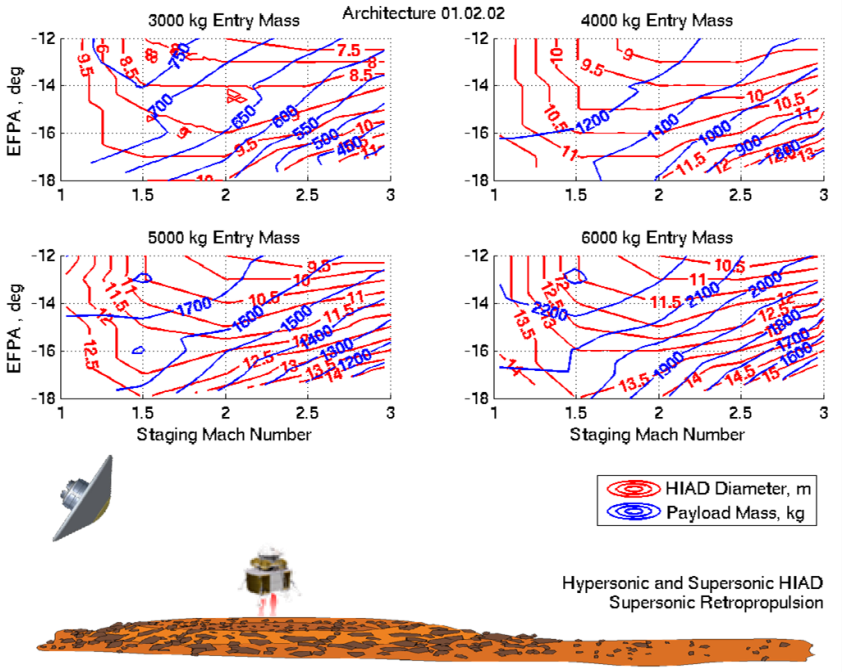

Figure 14. HIAD Diameter and Payload Mass Results.

IV. Summary of Relevant Scales

Each of the studies described in Section III provides insight into the size of the HIAD required in order to perform specific missions or classes of missions. A specific recommended HIAD scale was identified in consideration of mission objectives as well as performance and operational limits. For example, when looking at the Mars Southern Highlands study (Section III.E.3), a HIAD of roughly 15-meters enables EDL operations which require no supersonic staging events, while capable of delivering a payload to the surface comparable to an MSL class mission. At that scale, peak heat rate of the trajectory is not a driver. That is not the case for other studies, such as the L2 to LEO Transfer study (Section III.D.2), where heat rate is a driving factor. Assuming a 3rd generation flexible TPS, with a heat rate target of 75 W/cm^2, a HIAD of 23 meters is required in order to enable the hybrid entry vehicle to aerocapture a LEO orbit. Applying the target 3rd generation TPS performance across all studies results in the summary tabulated in Table 7.

Table 7. Recommended HIAD scale (75 W/cm^2 heat rate limit).

Study	Details	Entry Velocity	Entry Mass	Recommended Scale	Ballistic Coefficient
		[km/s]	[MT]	[m]	[kg/m2]
Launch Asset Recovery	2nd Stage Recovery	7.7	4	5	140
Launch Asset Recovery	1st Stage Recovery	3.5	22	10	200
Mars Aerocapture	Aerocapture 500 km circular orbit, L/D = 0.2	7.4	10.5	9	141
Mars Aerocapture	Aerocapture 500 km circular orbit, L/D = 0.2	9.5	14	26	23
Mars Southern Highlands	HIAD to supersonic/subsonic retro-propulsion	5.8	4	10	37.8
Mars Southern Highlands	HIAD to subsonic retro-propulsion	5.8	4	15	17
Hybrid Lunar Return	Hybrid Lunar return, direct entry	11	10.8	18	33
Mars Fast Transit	400 km circular orbit capture at Earth, L/D = 0.2	12	7	21	17.5

Mars Fast Transit	400 km circular orbit capture at Earth, L/D = 0.2	12	14	27	20
L2 to LEO Transfer	Hybrid L2 to LEO aerocapture, L/D = 0.2	11.5	11.5	23	24

It is important to note that ballistic coefficient reduces asymptotically with HIAD diameter and that peak heat rate effectively reduces linearly with reducing ballistic coefficient. Therefore, as the scale of the HIAD increases, it becomes increasingly difficult to deliver incremental reduction in peak heat rate. This is evident in the sensitivity of study results to assumed heating. For example, if peak convective heat rate is reduced by 50%, which is a rough proxy for the effects of a non-catalytic TPS material versus a super-catalytic material, one sees a greater reduction in recommended scale for the larger HIADS, particularly for those missions dominated by convective heating. This sensitivity is evident in Table 8.

Table 8. Sensitivity of recommended HIAD scale to aeroheating.

				Super-catalytic	**Non-catalytic**
Study	**Details**	**Entry Velocity**	**Entry Mass**	**Recommended Scale**	**Recommended Scale**
		[km/s]	**[MT]**	**[m]**	**[m]**
Mars Aerocapture*	Aerocapture 500 km circular orbit, L/D = 0.2	7.4	10.5	9	6
Mars Aerocapture*	Aerocapture 500 km circular orbit, L/D = 0.2	9.5	14	26	18
Hybrid Lunar Return	Hybrid Lunar return, direct entry	11	10.8	18	15
Mars Fast Transit	400 km circular orbit capture at Earth, L/D = 0.2	12	7	21	15
Mars Fast Transit	400 km circular orbit capture at Earth, L/D = 0.2	12	14	27	20
L2 to LEO Transfer	Hybrid L2 to LEO aerocapture, L/D = 0.2	11.5	11.5	23	16
* Run with non-catalytic aeroheating model, others studies employed 50% reduction in convective heating as a proxy					

V. Future Work

Year 2 of HIAD Mission Applications will focus on exploring additional mission classes as well as verify key Year 1 findings through more detailed design and analysis of specific reference missions. More specifically, Year 2 shall include the following activities:

- Investigate HIAD applicability to missions exploring alternative destinations including Venus, Titan and Uranus (aerocapture and direct entry studies)
- Complete a deep dive design cycle into select Mars Southern Highlands design points and update trade space models and recommended HIAD scale as appropriate
- Update mission application studies at Earth, Mars, Venus and Titan as dictated by model updates

VI. Conclusions

Systems analysis has demonstrated HIAD's to be applicable to a wide range of mission classes with potential benefits ranging from asset recovery, broader landing site access, simplified concept of operations, and reduced heating environments. Year 2 activities associated with HIAD Mission Applications will explore additional mission classes including destinations such as Venus, Titan and Uranus as well as verify potential benefits identified in Year 1 through detailed design and analysis of select reference missions. Sensitivity of the recommended HIAD scale grows with HIAD diameter, which needs to be considered during design and implementation. Further advances in flexible TPS technology as well as associated materials characterization could have a dramatic impact in reducing the recommended scale while expanding the range of applicable missions.

VII. References

[1] Hughes, Stephen, Cheatwood, Neil, Dillman, Robert, Wright, Henry, Del Corso, Joseph, Calomino, Anthony, "Hypersonic Inflatable Aerodynamic Decelerator Technology Overview", presented at the 21st Aero Decelerator Conference, AIAA 2011-2524.

[2] Samareh, J.A., and Komar, D.R., "Parametric Mass Modeling for Mars Entry, Descent, and Landing System Analysis Study," AIAA-2011-1038, 2011.

[3] Samareh, J.A., "Estimating Mass of Inflatable Aerodynamic Decelerators Using Dimensionless Parameters," 8th International Planetary Probe Workshop, June 6–10, 2011, Portsmouth, VA.

[4] Mazaheri, Alireza, "HEART Aerothermodynamic Analysis", NASA TM-20120217568.

[5] Wright, Henry, Cutright, Amanda, Corliss, James, Bruce, Walter, Trombetta, Dominic, Mazaheri, Alireza, Coleman, Michael, Olds, Aaron, Hancock, Sean, "HEART Flight Test Overview", presented at the 9th International Planetary Probe Workshop, Toulouse, France.

[6] Olds, Aaron D., Beck, Roger, Bose, David, White, Joseph, Edquist, Karl, Hollis, Brian, Lindell, Michael, Cheatwood, F.N., Gsell, Valerie, and Bowden, Ernest, "IRVE-3 Post-Flight Reconstruction", 22nd AIAA Aerodynamic Decelerator Systems Technology Conference, March, 2013.

[7] Cheatwood, F. M. and Gnoffo, P. A., "User's Manual for the Langley Aerothermodynamic Upwind Relaxation Algorithm (LAURA)," NASA TM 4674, April 1996.

[8] Gnoffo, P. A., Gupta, R. N., and Shinn, J. L., "Conservation Equations and Physical Models for Hypersonic Air Flows in Thermal and Chemical Nonequilibrium," NASA TP 2867, Feb. 1989.

[9] Johnston, C. O., Hollis, B. R., and Sutton, K., "Spectrum Modeling for Air Shock Layers at Lunar Return Conditions," Journal of Spacecraft and Rockets, Vol. 45, Sep.-Oct. 2008, pp. 865-878.

[10] Johnston, C. O., Hollis, B. R., and Sutton, K., "Non-Boltzmann Modeling for Air Shock Layers at Lunar Return Conditions," Journal of Spacecraft and Rockets, Vol. 45, Sep.-Oct. 2008, pp. 879-890.

[11] Johnston, C. O., Gnoffo, P. A., and Sutton, K., "Influence of Ablation on Radiative Heating for Earth Entry," Journal of Spacecraft and Rockets, Vol. 46, No. 3, 2009, pp. 481-491.

[12] Sutton, K., Hartung, L. C., "Equilibrium Radiative Heating Tables for Earth Entry," NASA TM 102652, May 1990.

[13] Hartung, L. C., Sutton, K., and Brauns, F., "Equilibrium Radiative Heating Tables for Aerobraking in the Martian Atmosphere," NASA TM 102659, May 1990.

[14] Tauber, M. E., and Sutton, K., "Stagnation-Point Radiative Heating Relations for Earth and Mars Entries," Journal of Spacecraft and Rockets, Vol. 28, No. 1, 1991, pp. 40-42.

[15] Park, C., "Review of Chemical-Kinetic Problems of Future NASA Missions, I: Earth Entries," Journal of Thermophysics and Heat Transfer, Vol. 7, pp. 385-398, 1993.

[16] Park, C., Jaffe, R.L., and Partridge, H., "Chemical-Kinetic Parameters of Hyperbolic Earth Entry," Journal of Thermophysics and Heat Transfer, Vol. 15, No. 1, pp. 76-90, 2001.

[17] Johnston, C. O., Mazaheri, A., Gnoffo, P. A., Kleb, B., Sutton, K., Prabhu, D., Brandis, A. M., and Bose, D., "Assessment of Radiative Heating Uncertainty for Hyperbolic Earth Entry," AIAA Paper 2011-3145, June 2011.

[18] Johnston, C. O., Brandis, A. M., and Sutton, K., "Shock Layer Radiation Modeling and Uncertainty for Mars Entry," AIAA Paper 2012-2866, June 2012.

[19] Komar, D.R., Hoffman, J., and Olds, A., "Framework for the Parametric System Modeling of Space Exploration Architectures," AIAA-2008-7845, 2008.

[20] Dwyer Cianciolo, A. M., et al. "Entry, Descent and Landing Systems Analysis Study: Phase 1 Report." NASA/TM-2010-216720.

[21] Heinemann, W., "Design Mass Properties II: Mass Estimating and Forecasting for Aerospace Vehicles Based on Historical Data," JSC-26098, November 1994.

[22] Press Kit, "Phoenix Landing: Mission to the Martian Polar North", National Aeronautics and Space Administration, May 2008.

[23] Tutt, B., Sandy, C., and Corliss, J., "Status of the Development of an Airbag Landing System for the Orion Crew Module," AIAA-2009-2923, 2009.

[24] Manders, R., "Apollo 11 Entry Post-flight Analysis", MSC Internal Note No. 70-FM-30, February 20, 1970.

[25] Malin, M. a., "Evidence for Recent Groundwater Seepage and Surface Runoff on Mars", Science, 288, 2330-2335, June, 2000.

[26] Braun, R. a., "Mars Exploration Entry, Descent and Landing Challenges", IEEE Aerospace Conference. Big Sky, MT, 2006.